Received 5 January 2022; revised 30 January 2022; accepted 31 January 2022. Date of publication 9 February 2022; date of current version 21 February 2022.

Digital Object Identifier 10.1109/OJAP.2022.3150094

Broadband Circularly Polarized Microstrip Patch Antenna With Diamond-Shaped Artificial Ground Structure

UUGANBAYAR PUREVDORJ (Graduate Student Member, IEEE), RYUJI KUSE (Member, IEEE), AND TAKESHI FUKUSAKO (Senior Member, IEEE)

Department of Computer Science and Electrical Engineering, Kumamoto University, Kumamoto 860-8555, Japan

CORRESPONDING AUTHOR: U. PUREVDORJ (e-mail: p.uuganbayar@must.edu.mn)

This work was supported by the Mongolia–Japan Higher Engineering Education Development (MJEED) Project (research profile code: J23A16).

ABSTRACT This paper presents a broadband circularly polarized patch antenna with an artificial ground structure (AGS), which has rotated rectangular unit cells with respect to the sides of the rectangular ground plane, as a polarizer. A two-element (2×1) array configuration of the antenna is also presented. The rectangular unit cells are rotated by 45° with respect to the sides of a square dielectric substrate, named a diamond-shaped AGS (DAGS). The overall dimensions of the AGS are smaller than those of the ground plane. The rotated unit cells and the smaller AGS patch dimensions effectively suppress surface wave resonance on the AGS. The proposed antenna achieves a wide 3-dB axial ratio bandwidth in the boresight direction. The proposed design has a flatter gain curve in the operating frequency band compared to that for conventional designs. It is found that the array configuration outperforms the single-element structure.

INDEX TERMS Artificial ground structure (AGS), artificial magnetic conductor (AMC), broadband antenna, circular polarization, meta-surface, microstrip patch antenna, microstrip patch array antenna.

I. INTRODUCTION

THE DESIGN of circularly polarized broadband antennas has received a lot of research attention [1]. Patch antennas, which can be circularly polarized using various techniques, have several advantages, such as low cost, low profile, ease of fabrication [2] and many applications such as satellite communications, radars, GNSS and WLAN. However, microstrip patch antennas have relatively narrow impedance and 3-dB axial ratio (AR) bandwidths. Artificial ground structures (AGSs), which act as an artificial magnetic conductor and a polarizer, have been proposed for achieving broadband circular polarization (CP) and impedance for patch antennas [3]–[17]. In conventional AGSs, rectangular unit cells are arrayed periodically so that their sides are parallel to the sides of a grounded rectangular substrate. However, based on an analysis of magnetic currents between unit cells, unwanted resonances related to the paths with various lengths of the magnetic current between the unit-cell array or a side of the ground plane disturbs the relationship for the CP of the two orthogonal components $|E_x| = |E_y|$ with a 90° phase difference, limiting wideband 3-dB AR. Thus, the dependence of the AGS characteristics on the geometry of the ground plane and the dimension of the unit-cell array should be taken into account. A modified rotated AGS, where the rectangular unit cells are rotated by 45° with respect to the sides of the rectangular ground plane, named a diamond-shaped AGS (DAGS), was developed to reduce the unwanted resonances that affect the broadband CP characteristics [7], [19]. The unwanted resonances in a DAGS are weak because the resonance of the magnetic current, which depends on the rows and columns, is spread over several frequencies.

In this paper, a DAGS is installed in a circularly polarized patch antenna. First, the characteristics of a DAGS are compared with those of an AGS, for which the sides of the unit cell are parallel to those of the rectangular ground plane. Then, improvements in patch antennas for achieving wider bandwidths and stable gain characteristics

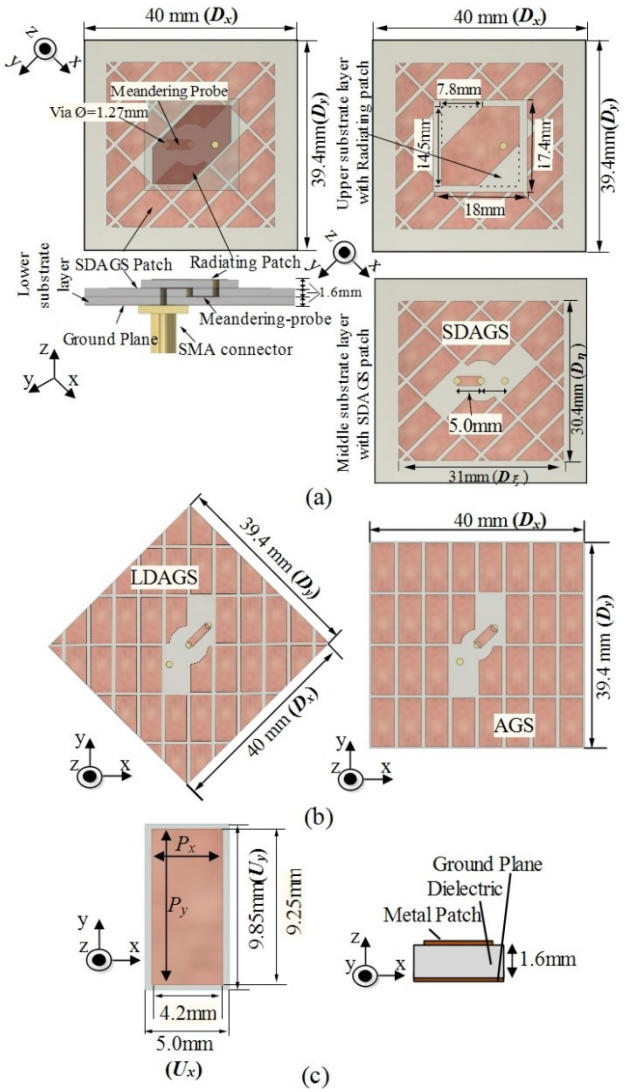

FIGURE 1. (a) Top and side views of proposed antenna with SDAGS. (b) Structures used for comparison (LDAGS and AGS). (c) Unit cell configuration for (a) and (b).

are discussed. A patch array antenna on a common ground plane and a substrate with a DAGS are proposed and discussed. Simulation results are verified by experiments. The mechanisms responsible for the observed improvement are discussed.

II. SINGLE ANTENNA STRUCTURE

A DAGS is designed to have ±90° reflection phase shifts of the x and y components of the electric field, E_x and E_y, respectively, at around 6 GHz to convert elliptical polarization to CP in the off-band of the 3-dB AR [14]. The geometry of the proposed antenna structure with the DAGS is shown in Fig. 1(a), where the DAGS patch dimension is reduced from the ground plane to be a smaller DAGS(SDAGS). This area reduction of the DAGS patch layer leads to stable CP characteristics, as discussed later.

The proposed antenna consists of three stacked substrates, namely an upper substrate with a radiating patch, a middle substrate with DAGS patches, and a lower grounded substrate.

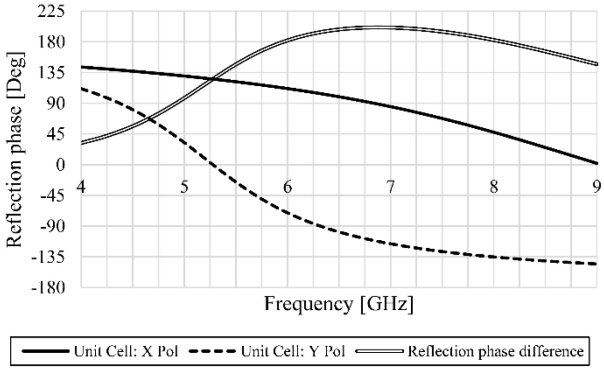

FIGURE 2. Reflection phases and phase difference for unit cell.

The patch antenna is fed with a meandering feed probe [20], [21] to reduce cross-polarization. The rectangular unit cells are rotated by 45° with respect to the sides of the ground plane. The lower and middle substrates and the ground plane have overall dimensions $D_x \times D_y = 40$ mm × 39.4 mm. The SDAGS has reduced dimensions of $D_\xi \times D_\eta = 31$ mm × 30.4 mm. The upper substrate underneath the radiating patch has dimensions of 18 mm × 17.4 mm for obtaining stable antenna gain characteristics. The radiating patch has a rectangular shape with dimensions of 14.5 mm × 14.5 mm and two truncated corners with dimensions of 7.8 mm × 7.8 mm for radiating CP.

The antenna is fed by a single meandered feed line. Two of the unit cells around the center of the DAGS are partially drilled, and two other unit cells near the feed line are fully removed to prevent the meandering probe from coupling with the unit cells. The diameter of the vias is 1.27 mm. The feeding point of the radiating patch is 5 mm from the center of the truncated patch along the x axis for sufficient impedance matching and AR over a broad bandwidth. Furthermore, the unit cells are partially (some are mostly) cut around the edges of the DAGS to be along the rectangular contour. Here, the optimized size of the DAGS patch is smaller than those of the dielectric substrates and the ground plane.

The characteristics of the antenna are compared with those of reference structures, namely the larger DAGS (LDAGS) and AGS shown in Fig. 1(b). The spatial relationship between the radiation patch and the rectangular AGS patches is the same. In the DAGS (LDAGS and SDAGS), only the relationship between the DAGS outer contour and each rectangular patch has been changed compared to the AGS. The optimized dimensions of the unit cell are shown in Fig. 1(c). The unit cell is 5.00 mm × 9.85 mm on the substrate, and the patch of the unit cell is 4.20 mm × 9.25 mm. A 1.6-mm-thick RT/Duroid 5880 substrate is used for all three substrates in the proposed antenna.

Fig. 2 shows the phase shift characteristics of the rectangular unit cell of the DAGS shown in Fig. 1(c), where

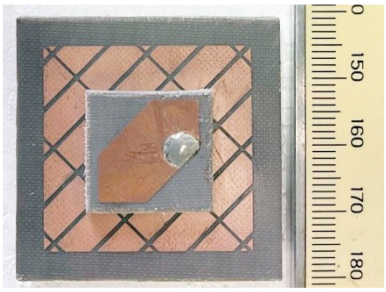

FIGURE 3. Photograph of fabricated antenna with proposed SDAGS.

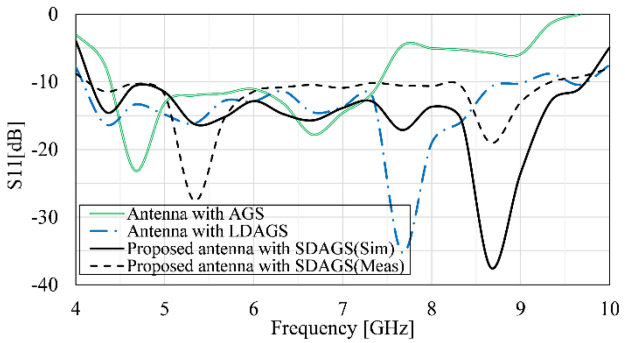

FIGURE 4. Simulated reflection coefficients for structures with AGS and LDAGS, respectively, compared to simulated and measured S_{11} for proposed antenna with SDAGS.

periodic boundary conditions are applied to each unit cell in ANSYS High Frequency Structure Simulator (HFSS). The structure converts linear polarization to CP with $+90°$ and $-90°$ reflection phases for E_x and E_y around 6 GHz [14]. A deviation of up to 20° from a phase difference of 180° between E_x and E_y is observed at 5.50–8.50 GHz; however, this is acceptable for AR $\leq$ 3 dB if $|E_x| = |E_y|$ is assumed.

III. EFFECT OF DAGS

A. ANTENNA CHARACTERISTICS

The performance of the antenna with an SDAGS (31 mm × 30.4 mm) is compared with that of an antenna with an LDAGS (40 mm × 39.4 mm) with the unit cell dimensions shown in Figs. 1(a) and 1(b), respectively. The performance obtained with an SDAGS is also compared with that obtained with an AGS, where the sides of the unit cells are parallel to those of the substrates and ground plane, as shown in Fig. 1(b). The proposed antenna structure was fabricated and tested to verify the simulation results. Its characteristics and radiation pattern were measured.

All metallic patterns were fabricated by the RT/Duroid 5880 dielectric substrate material using etching technique. Fig. 3 shows a photograph of the fabricated antenna.

Fig. 4 shows a wider −10-dB S11 bandwidth of 74.39% (from 4.12 to 9.00 GHz) for the SDAGS in the simulation; it is almost identical to that obtained with the LDAGS. The −10-dB bandwidth for both DAGSs is considerably wider than that for the AGS.

As shown in Fig. 4, the simulated and measured impedance bandwidths for the proposed antenna with an SDAGS ($|S11| \leq -10$ dB) are 79.71% and 76.57% in the frequency ranges of 4.21–9.79 GHz and 4.15–9.30 GHz, respectively, with good agreement.

The far-field simulations performed by radiation boundary in open region boundary conditions in HFSS.

Fig. 5(a) shows the simulated AR characteristics in the $+z$ direction for antennas with a conventional ground plane (without AGS, where unit cells are removed from the AGS), AGS, LDAGS, and SDAGS, and the measured AR characteristics of the proposed antenna with SDAGS. For the AGS, the 3-dB AR bandwidth of more than 20% is wider than the bandwidth for the structure with a ground plane [1], [14]–[15]. However, the extra resonances of the $TM_{(x)}$ mode with $D_x = 40.0$ mm in Fig. 1(b), which is along the x-direction in the AGS, limit the expansion of the 3-dB AR bandwidth around 7 GHz [16]. When an LDAGS or SDAGS is used, the strong resonance at 7 GHz is decreased. Therefore, the 3-dB AR bandwidths in the boresight direction are broadened in the antennas with the LDAGS and SDAGS. Simulated 3-dB AR bandwidths of 40.7% (from 5.40 to 8.16 GHz) and 37.3% (from 5.00 to 7.30 GHz) are obtained for the SDAGS and LDAGS, respectively. The simulated and measured 3-dB AR bandwidths for SDAGS show good agreement, with (AR $\leq$ 3 dB) 3-dB AR bandwidths of 40.7% and 41.2% for 5.40–8.16 and 5.45–8.28 GHz, respectively, as shown in Fig. 5(a). In Figs. 5(b) and 5(c), the amplitude ratio and phase difference do not satisfy the condition for a CP of 0 dB and 90° simultaneously at 6.25, 7.00, and 7.71 GHz for the structures with the AGS and LDAGS. The mechanism producing the resonances at these three frequencies (deterioration frequencies) is discussed in the following subsection.

Furthermore, as shown in Fig. 6, the gain of the SDAGS is stable over the 3-dB AR band and is improved compared to that of the AGS, especially at high frequency. The mechanism responsible for this improvement is discussed in the next subsection.

In the figure, the simulated and measured results show good agreement in the 3-dB AR band, with maximum gains of 8.82 and 8.75 dBic, respectively, at around 6.85 GHz. The simulated and measured bandwidths of the 3-dB gain variation are 4.3–10.2 GHz (81.37%) and 4.9–10.4 GHz (71.89%), respectively.

B. ANALYSIS OF RESONANCE IN DAGS

In the AGS or DAGS, linear polarization (LP) or high-AR polarization can be potentially converted to circular polarization in the frequency where the difference of reflection phase shift between x- and y-components in Fig. 2 is close to 180° [14]. As the effect of the extra resonances has become weak, the x- and y-components can be balanced for CP generation. The weaken resonance is due to that the electromagnetic energy in the DAGS has been spread in several resonances with various path lengths of magnetic

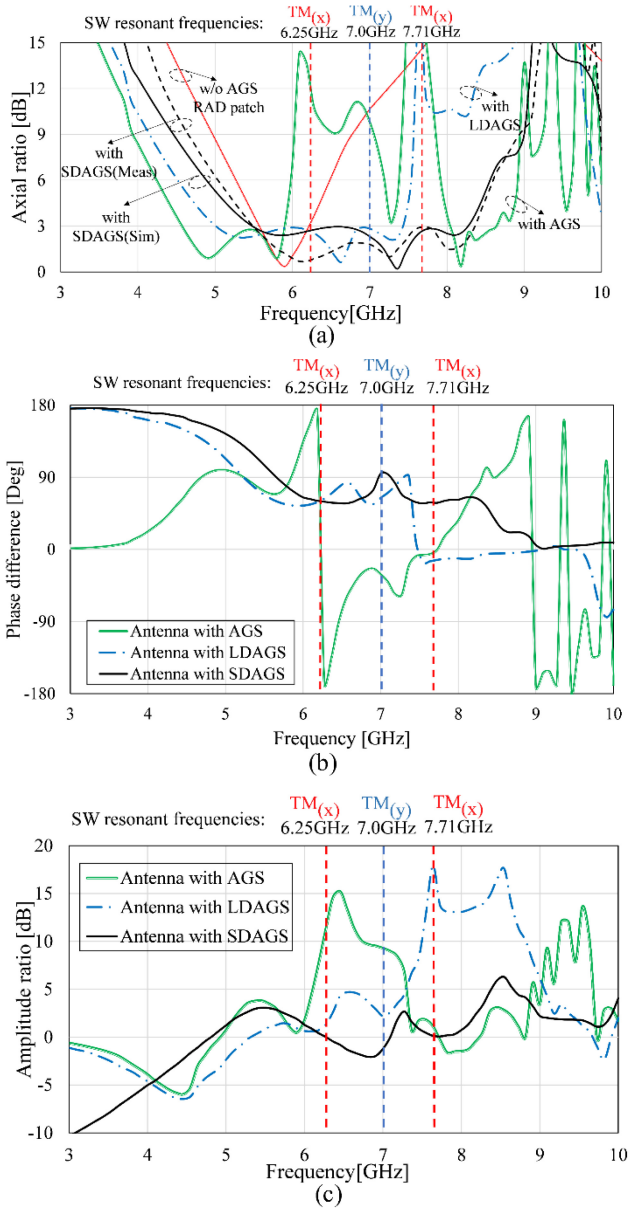

FIGURE 5. Simulated (a) AR characteristics (along with measurement results) in +z direction of structures, (b) amplitude characteristics of $|E_X|/|E_Y|$, and (c) phase difference characteristics for Arg E_X-Arg E_Y for structures without AGS (unit cells removed) and with AGS, LDAGS, and SDAGS.

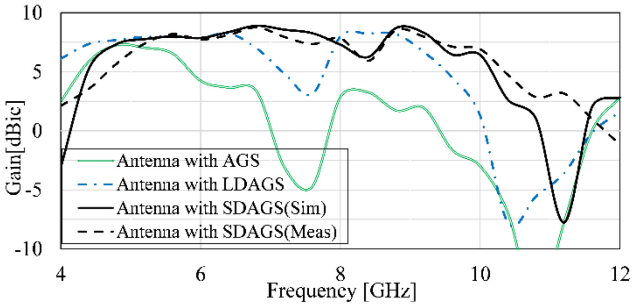

FIGURE 6. Simulated gain characteristics in +z direction for structures with AGS and LDAGS, compared to simulated and measured gains for proposed antenna with SDAGS.

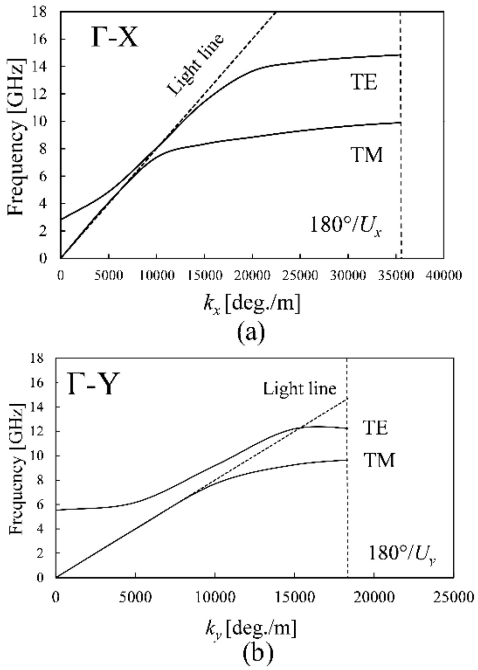

FIGURE 7. Dispersion diagrams. U_X and U_Y are unit cell sizes along x and y directions, respectively.

current resulting in the low energy density at each resonance frequency. To analyze the resonance mechanism, the dispersion characteristics for an infinite unit cell of an AGS were calculated.

Fig. 7 shows dispersion diagrams for the unit cell in Fig. 1(c) for transverse electric (TE) and (transverse magnetic) TM modes in the x and y directions calculated based on an eigenmode analysis using periodic boundary conditions for the HFSS [18]. These diagrams show the relationship between the propagation constant and the frequency for the $\Gamma-X$ and $\Gamma-Y$ directions of the first Brillouin zone in wavenumber space. For resonance along x and y, the propagation constants k_i ($i = x$ or y) satisfy the following condition:

$$k_i D_i = n \times 180^\circ \tag{1}$$

where n is an integer that indicates the resonance order.

The calculated resonance frequencies are summarized in Table 1. It is known that the TM mode plays a dominant role in an AGS [6]. According to Table 1, the resonance frequencies for the TM mode for an AGS ($D_x \times D_y$ = 40 mm × 39.4 mm) are at 6.25 and 7.71 GHz in the x direction and at 7.00 GHz in the y direction in the 3-dB AR band.

Fig. 5(a)−(c) shows the effect of resonance. The AR obtained with an AGS exceeds 3 dB and leads to a peak at high values for deterioration frequencies of 6.25, 7.00, and 7.71 GHz in $TM_{(x)}$ mode with D_x = 40 mm, as indicated by the vertical dashed lines. Therefore, a narrow AR bandwidth (∼23%) is observed for an antenna with an

TABLE 1. TM and TE mode resonance frequencies for AGS in X and Y directions.

Direction	x-direction (D_x=40mm)		y-direction (D_y=39.4mm)	
Modes	TE	TM	TE	TM
Resonant Frequency (GHz)	4.55	3.62	5.86	3.68
	7.26	**6.25**	8.04	**7.00**
	10.15	**7.71**	11.39	8.65
		8.54	12.09	9.65
		9.1		
		9.45		

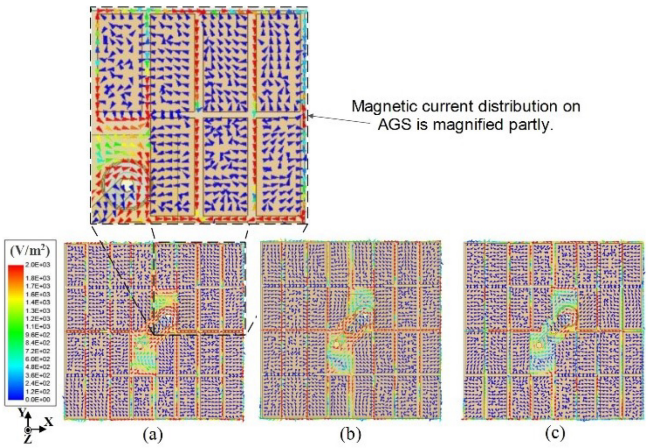

FIGURE 8. Simulated magnetic current distributions for AGS at (a) 6.25, (b) 7.0, and (c) 7.71 GHz.

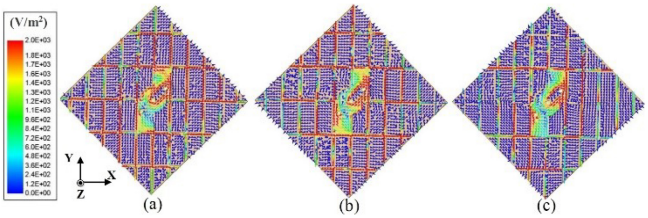

FIGURE 9. Simulated magnetic current distributions for LDAGS at (a) 6.25, (b) 7.0, and (c) 7.71 GHz.

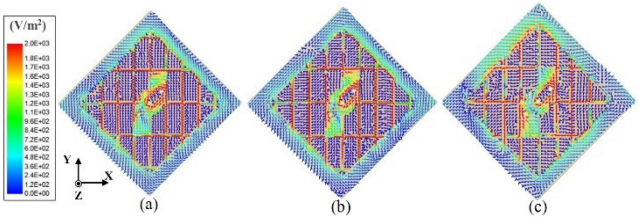

FIGURE 10. Simulated magnetic current distributions for SDAGS at (a) 6.25, (b) 7.0, and (c) 7.71 GHz.

TABLE 2. Amplitude ratio and phase difference for magnetic current.

Deterioration points		6.25 GHz	7 GHz	7.71 GHz
AGS	$\lvert E_X\rvert/\lvert E_Y\rvert$ [dB]	-15.23	-5.25	-3.13
	PD [°]	175.16	-127.46	-62.38
LDAGS	$\lvert E_X\rvert/\lvert E_Y\rvert$ [dB]	-2.16	0.56	11.44
	PD [°]	57.67	105.05	19.91
SDAGS	$\lvert E_X\rvert/\lvert E_Y\rvert$ [dB]	-2.60	-0.44	-0.93
	PD [°]	89.49	119.47	80.02

AGS [1], [14]−[15]. In terms of the bandwidth, the phase differences at the deterioration frequencies are not close to 90°, the condition required for generating CP, as shown in Fig. 5(b).

The peaks of ∼15 dB and ∼10 dB are observed at resonance frequencies of 6.25 and 7.00 GHz in amplitude ratio response. These high amplitude ratios exceed the condition for CP of 0 dB. At 7.71 GHz, the amplitude ratio satisfies this condition; however, the only phase difference is far from the condition, as shown in Fig. 5(c). For the proposed structure with an SDAGS, such resonances at the deterioration frequencies are not observed. According to Fig. 5(a)−(c), the 3-dB AR bandwidth is expanded up to 40.7% (5.40−8.16 GHz).

As described above, the AR is deteriorated in an AGS due to resonances at some frequencies; however, a DAGS can suppress these extra resonances. To determine the mechanism involved, simulated magnetic current distributions between the unit cells (copper) on the substrate surface of the AGS, LDAGS, and SDAGS were observed [7], [22], [23] at the deterioration frequencies.

As shown in Fig. 8 for the AGS, the magnetic current along the y direction is stronger than that along the x direction for all deterioration frequencies. This indicates that E_x is stronger than E_y and explains the behavior shown in Fig. 5(c). Therefore, the 3-dB AR bandwidth is limited to ∼23%, and the AR increases at the deterioration frequencies, as shown in Fig. 5(a).

At the same time, a strong magnetic current is observed around the center and along the edge of the AGS.

The use of a DAGS can balance the magnetic currents between the x and y directions to satisfy the condition required for CP. The magnetic current distributions at the deterioration frequencies for the LDAGS and SDAGS are shown in Figs. 9 and 10, respectively.

In both structures, the strength of the magnetic current is balanced in the x and y directions. Moreover, strong magnetic currents are mitigated along the edges due to the effect of the partially cut unit cells along the contours of the DAGSs [7].

The amplitude ratio and phase difference for the magnetic currents in the x and y directions were evaluated numerically at the resonance frequencies for the AGS, LDAGS, and SDAGS.

The amplitude ratio (X/Y) and phase difference (PD) were calculated using surface integration in HFSS. The results are shown in Table 2. For the AGS, the amplitude ratio and phase difference are not close to the condition, i.e., $|E_X|/|E_Y|$ is 0 dB and PD = 90°, required for CP at any frequency. Therefore, the phenomenon in AGS as shown in Fig. 8 is proved.

For the LDAGS, the conditions are almost satisfied at 6.25 and 7.00 GHz but not at 7.71 GHz, resulting in a 3-dB AR bandwidth of up to 37.3%. For the SDAGS, the amplitude

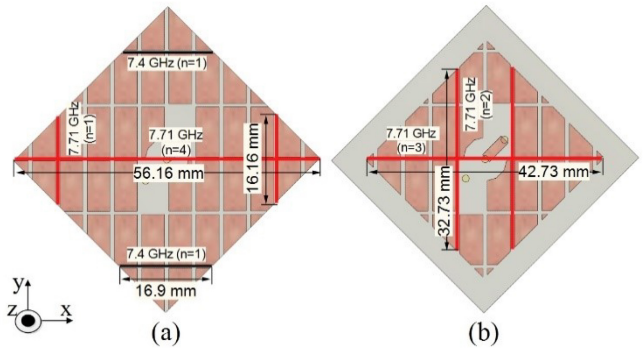

FIGURE 11. Simulated magnetic current distributions for LDAGS at (a) 6.25, (b) 7.0, and (c) 7.71 GHz.

TABLE 3. TM mode resonance frequencies for possible paths of LDAGS and SDAGS around deterioration point at 7.71 GHZ and amplitude ratio for magnetic current.

Structure	LDAGS			SDAGS	
Axis	X	X	Y	X	Y
Length [mm]	16.9	56.16	16.16	42.73	32.73
n	1	4	1	3	2
Frequency	7.4 GHz	7.71 GHz	7.70 GHz	7.72 GHz	7.70 GHz
$\lvert E_X\rvert/\lvert E_Y\rvert$ [dB]		-14.22		-1.74	

ratio and phase difference are close to those required at all three frequencies. Accordingly, the DAGSs can balance magnetic currents in the x and y directions as a same to explanations in Figs. 9 and 10.

The behavior of the resonance at 7.71 GHz in both the LDAGS and SDAGS was analyzed along the paths with various lengths of the magnetic current in the x and y directions. The results are shown in Fig. 11; Table 3 shows the resonance frequencies for various lengths and corresponding orders n. In the LDAGS, the resonances are at 7.4 and 7.71 GHz in the x direction for magnetic current paths with lengths of 16.9 mm ($n = 1$) around two corners (top and bottom) and 56.16 mm ($n = 4$) along the horizontal diagonal. Similarly, in the y direction, the resonance is at 7.7 GHz for a path with length of 16.16 mm ($n = 1$) around the other two corners. In the SDAGS, the resonance is at around 7.7 GHz in both the x and y directions for paths with lengths of 42.73 mm ($n = 3$) and 32.73 mm ($n = 2$), respectively.

For the LDAGS, with increasing frequency, the magnetic current tends to be distributed mainly around the feed probe structure, as shown in Fig. 9, resulting in a biased magnetic current distribution. Resonance was expected at 7.71 GHz with $n = 4$, as shown in Fig. 11(a); however, resonance for the long length was not confirmed, as shown in Fig. 9(c). In addition, the resonance with $n = 1$ is very weak. The amplitude ratio for the magnetic current at 7.71 GHz along the possible paths with resonance in the x and y directions were evaluated numerically using surface integration in HFSS. The calculated amplitude ratio between the fourth-order resonance in the x direction and the first-order resonance in the y direction at 7.71 GHz is not satisfied for a CP wave by -14.22 dB, as shown in Table 3.

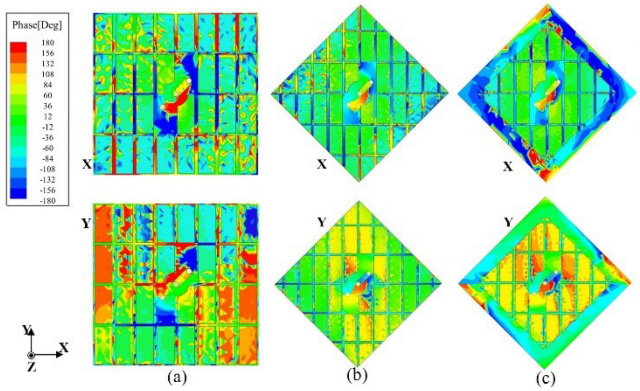

FIGURE 12. Phase distributions in x and y directions at 7.0 GHz in (a) AGS, (b) LDAGS, and (c) SDAGS.

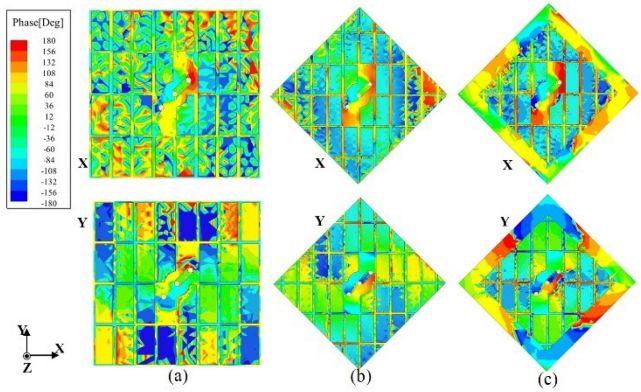

FIGURE 13. Phase distributions in x and y directions at 7.71 GHz in (a) AGS, (b) LDAGS, and (c) SDAGS.

For the SDAGS, according to Table 3, the amplitude ratio for the magnetic current at 7.71 GHz is balanced to an acceptable level of -1.74 dB for CP radiation in the proposed antenna. This leads to an expansion of the 3-dB AR bandwidth to 40.7% with the SDAGS. This is partly due to the resonance can occurs with the paths in Fig. 11(b). In addition, the distribution is more uniform because the area of the unit-cell array is limited compared to that for the LDAGS.

The gain for antennas with both DAGSs (LDAGS and SDAGS) was relatively stable and higher than that for the antenna with an AGS, as shown in Fig. 6. The gain obtained with an AGS significantly drops around 7.0 and 7.71 GHz. The gain is improved via resonance suppression for both DAGSs.

These stable characteristics can be explained by the uniform magnetic current distribution between unit cells, as shown in Figs. 8–10, where a very small amplitude of the magnetic current can be observed underneath the copper patches of the unit cell. Among the three structures, the most uniform distribution of the magnetic current between the unit cells in the x and y directions is obtained with the SDAGS at deterioration frequencies of 7.0 and 7.71 GHz, as shown in Figs. 8 and 9, respectively.

In Figs. 12 and 13, the phase varies from $-180°$ to $+180°$ in the AGS at both frequencies. Therefore, cancellation via

TABLE 4. Simulated and measured radiation characteristics of proposed CP microstrip patch antenna.

Frequency [GHz]	XPL [dB]				FB ratio [dB]				HPBW[Deg]			
	XZ-plane		YZ- plane		XZ-plane		YZ- plane		XZ-plane		YZ- plane	
	Sim.	Meas.	Sim.	Meas.	Sim	Meas.	Sim.	Meas.	Sim	Meas.	Sim	Meas.
5.5	-13.57	-16.33	-13.57	-22.74	24.15	22.27	25.77	24.29	67.5	75	65	72.5
6.0	-15.94	-18.75	-15.94	-20.59	25.47	27.4	25.29	25.68	65	63	62.5	70
6.5	-15.80	-22.36	-15.80	-16.68	20.33	29.39	20.33	20.92	67.5	85	60	80
7.25	-24.47	-22.14	-24.47	-22.49	19.17	17.83	21.06	15.31	60	60	60	50
8.0	-14.91	-18.94	-14.91	-17.59	18.84	18.18	19.05	22.67	57.5	55	57.5	57.5

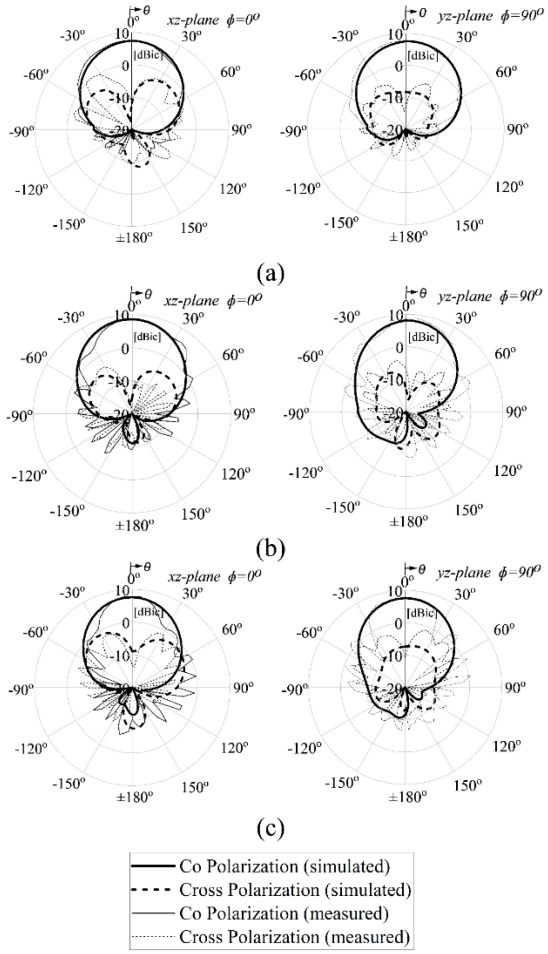

FIGURE 14. Simulated and measured co- and cross-polarization radiation patterns in *x-z* and *y-z* planes for proposed antenna at (a) 6.0, (b) 7.25, and (c) 8.0 GHz.

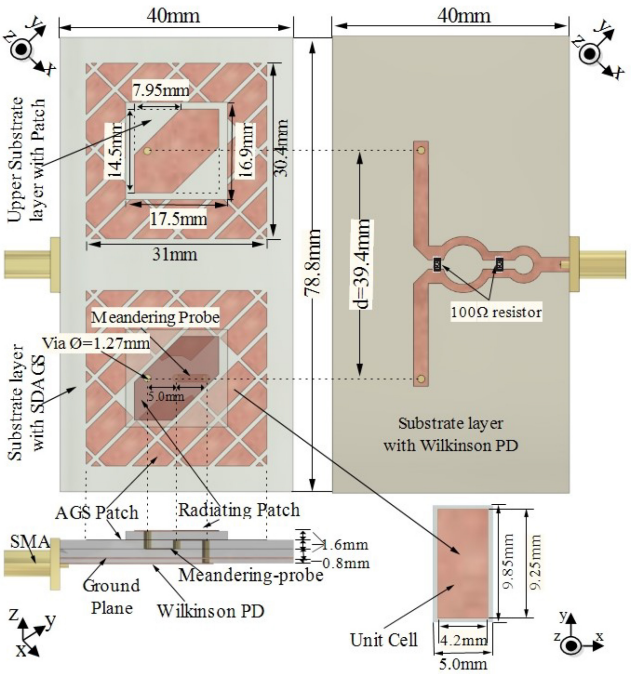

FIGURE 15. Two-element array structure of proposed CP antenna.

phase variation explains the gain reduction at the deterioration frequencies. The LDAGS shows a smaller phase variation than that of the AGS, whereas the SDAGS shows a 90° phase difference between the x and y directions with a more uniform distribution. than those for the LDAGS and AGS at the two frequencies.

This also explains the stable gain characteristics of the antenna with the SDAGS. It was also observed that cross-polarization was sufficiently suppressed.

Fig. 14 shows that the simulated and measured radiation patterns have good agreement in the x-z and y-z planes at 6.0, 7.25, and 8.0 GHz. In this structure, the radiation pattern is a composite result from the patch elements and the DAGS.

Table 4 summarizes the simulated and measured radiation characteristics of the proposed CP microstrip patch antenna with the SDAGS.

Table 5 compares the overall performance of the proposed CP antenna with that of existing metasurface-based single-fed CP microstrip antennas in terms of the -10-dB impedance bandwidth, 3-dB AR bandwidth, 3-dB gain bandwidth, maximum gain, and overall antenna dimensions. The proposed antenna with the SDAGS has the widest fractional bandwidths of $|S11| \leq -10$ dB (76.57%) and 3-dB gain variation (71.89%).

The proposed antenna also achieves comparable results in terms of the bandwidth of AR $\leq$ 3 dB (42.75%) and maximum gain (8.75 dBic) while having a lower profile and more compact dimensions.

In addition, the 3-dB AR band is included in the bandwidths of the 3-dB gain and -10-dB $|S11|$.

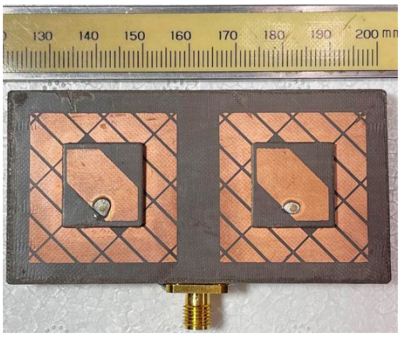

FIGURE 16. Photograph of fabricated antenna with two-element array.

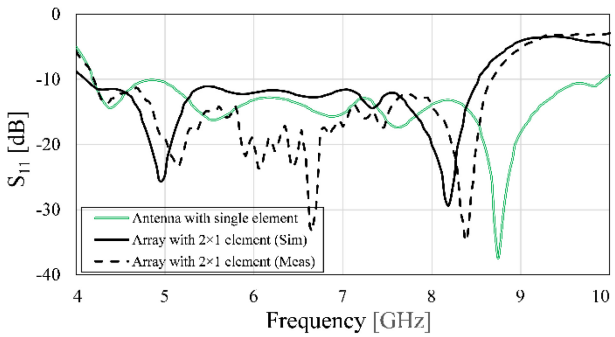

FIGURE 17. Simulated and measured S11 characteristics of array antenna and simulated S_{11} characteristics of single-element structure.

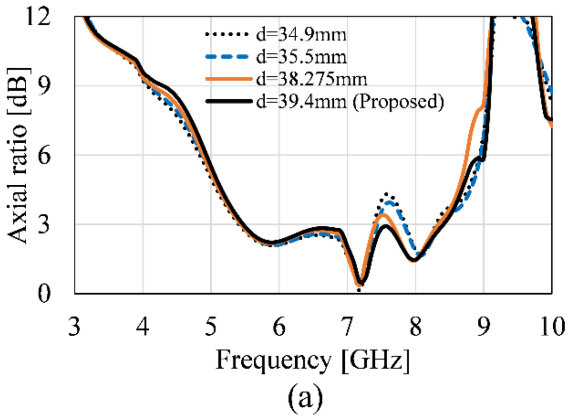

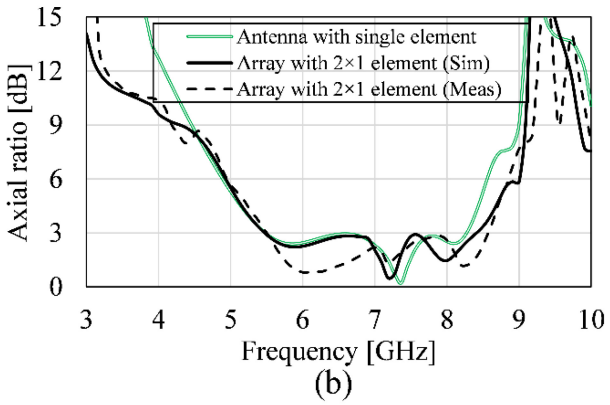

FIGURE 18. AR characteristics in $+z$ direction for array structure. (a) Results of parameter study and (b) comparison to single-element structure and experimental results.

IV. ARRAY CONFIGURATION

Patch antennas are often arrayed on a substrate and a ground plane [4], [5]. Because the characteristics of the AGS are affected by the size of the ground plane and the AGS patch, an array structure with a DAGS on a shared substrate and a ground plane was investigated.

A patch antenna with a two-element array structure based on SDAGSs was examined, as shown in Fig. 15, where an additional substrate layer of the Wilkinson power divider is used for a branched feeding line underneath the ground plane. The simulation results for the array design were validated by measurements of the prototype antenna shown in Fig. 16 using the same substrate (RT/Duroid 5880) as that in the single-element structure.

Fig. 17 shows the simulated and measured |S11| characteristics for the proposed array antenna compared to those for a single-element structure. The simulated −10-dB |S11| bandwidth is 68% ranging from 4.18 to 8.5 GHz. Fig. 18(a) shows the AR characteristics in the boresight direction for several values of d. When $d < 39.4$ mm, a small AR peak at around 7.5 GHz is observed. This is due to the effect of coupling between the two DAGSs. When $d \geq 39.4$ mm, the peak is less than 3 dB, and the 3-dB AR bandwidth for the array is almost the same as that for the single-element structure, as shown in Fig. 18(b). We can conclude that only a small effect of the coupling is observed.

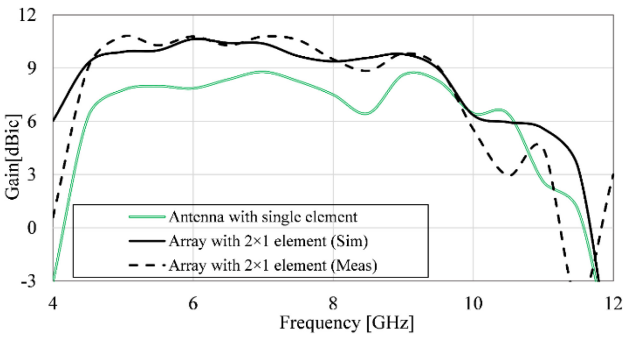

FIGURE 19. Simulated and measured gain characteristics of array antenna and simulated gain characteristic of single-element structure in $+z$ direction.

The simulation and measurement results almost overlap. A bandwidth of 43.7% is measured at 5.45−8.5 GHz.

Fig. 19 shows the simulated and measured gain characteristics in the $+z$ direction for the proposed array compared to those for the single-element structure. The gain of the array was increased by nearly 3 dB, as expected, compared to that for the single-element structure.

The simulated and measured maximum gains are 10.68 and 10.77 dBic, respectively, at around 6.00 GHz.

TABLE 5. Comparison of performance of proposed antenna and existing CP single-FED microstrip antennas with metasurfaces.

References	|S11| BW (%)	3-dB AR BW (%)	3-dB gain BW (%)	Maximum gain (dBic)	Overall Dimension
[1]	54.6	25.2	48.65	6.52	$0.607\lambda_L \times 0.623\lambda_L \times 0.083\lambda_L$ at 4.67GHz
[3]	36	28.3	40	7.4	$0.682\lambda_L \times 0.979\lambda_L \times 0.050\lambda_L$ at 3.32GHz
[10]	36.2	33.2	34.78	7	$0.605\lambda_L \times 0.504\lambda_L \times 0.160\lambda_L$ at 5.04GHz
[11]	45.6	23.4	36.36	7-7.6	$0.496\lambda_L \times 0.496\lambda_L \times 0.048\lambda_L$ at 4.7GHz
[12]	35	22	38.99	7.72	$0.873\lambda_L \times 0.655\lambda_L \times 0.052\lambda_L$ at 3.28GHz
[13]	40, 49.5	19.3, 33.8	66.67	7.4	$0.533\lambda_L \times 0.533\lambda_L \times 0.133\lambda_L$ at 2.0GHz
[14]	42	22	32	7.2	$0.606\lambda_L \times 0.621\lambda_L \times 0.082\lambda_L$ at 4.66GHz
[17]	47.82	43.81	60.47	9.74	$1.068\lambda_L \times 1.068\lambda_L \times 0.091\lambda_L$ at 5.17GHz
Proposed antenna	76.57	42.75	71.89	8.75	$0.623\lambda_L \times 0.613\lambda_L \times 0.083\lambda_L$ at 4.67GHz

λ_L is the free space wavelength of the lowest operating frequency.

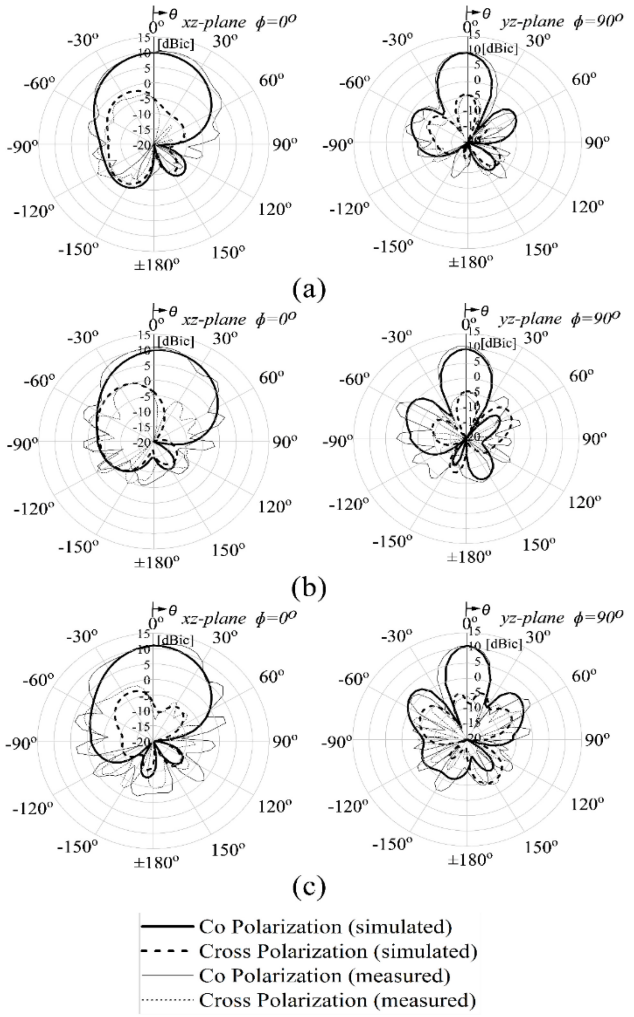

FIGURE 20. Simulated and measured co- and cross-polarization radiation patterns in *x-z* and *y-z* planes for proposed antenna with array at (a) 6.0, (b) 6.5, and (c) 7.25 GHz.

The simulated and measured bandwidths of the 3-dB gain variations of the array are 4.2−9.85 GHz (80.42%) and 4.25−9.80 GHz (79.00%), respectively.

Fig. 20 shows the simulated and measured radiation patterns in the $+z$ direction for the array design of the proposed CP antenna at the selected frequencies of 6.0, 6.5, and 7.25 GHz in the 3-dB AR band. There is good agreement between the simulation and measurement results. The cross-polarization was suppressed. The results indicate that the effect of coupling between the elements can be ignored.

V. CONCLUSION

A single-feed circularly polarized patch antenna with a DAGS was proposed. The diamond-shaped alignment avoids strong resonances of surface waves on the DAGS. The proposed structure, whose size is the same as that of an AGS antenna [1], achieves a 3-dB AR bandwidth of up to around 40% and stable gain characteristics. To achieve a broader 3-dB AR bandwidth, the SDAGS unit cell effectively suppressed the extra resonance that enhanced one of the orthogonal radiation components in the far field region. Furthermore, the smaller dimensions of the unit-cell array led to a uniform magnetic current distribution throughout the operating band with controlled resonance in the x and y directions at the relatively high frequency of the 3-dB AR band. This results in stable gain characteristics, especially at high frequencies. As an additional advantage in DAGS, we can mention that the AGS consisting of rectangular unit cells is rotated by 45° and the edges are simply cut diagonally and linearly to the sides of the rectangular unit cells, making it easy for fabrication. In addition, a two-element array configuration (2 × 1) for the proposed CP antenna with a SDAGS was presented. This array structure achieved a 3-dB AR bandwidth of 40% even though the two patch antennas were fabricated on a common ground plane and substrate. Coupling between the two DAGS unit-cell arrays should be avoided to reduce extra resonances.

The results show that the proposed structures are candidates for broadband CP applications. Reducing the coupling between the DAGS will be considered in a future study. Discussions using equivalent circuit would be an interesting future problem.

REFERENCES

[1] T. Nakamura and T. Fukusako, "Broadband design of circularly polarized microstrip patch antenna using artificial ground structure with rectangular unit cells," *IEEE Trans. Antennas Propag.*, vol. 59, no. 6, pp. 2103–2110, Jun. 2011.

[2] U. Purevdorj, R. Kuse, and T. Fukusako, "Broadband circularly polarized microstrip patch antenna using artificial ground structure with rotated rectangular unit cells," in *Proc. IEEE AP-S/URSI*, 2021, p. WE-A1.4P.3.

[3] N. Nasimuddin, Z. N. Chen, and X. Qing, "Bandwidth enhancement of a single-feed circularly polarized antenna using a metasurface: Metamaterial-based wideband CP rectangular microstrip antenna," *IEEE Antennas Propag. Mag.*, vol. 58, no. 2, pp. 39–46, Apr. 2016.
[4] S. X. Ta and I. Park, "Planar wideband circularly polarized metasurface-based antenna array," *J. Electromagn. Waves Appl.*, vol. 30, p. 1621, Jul. 2016.
[5] I. Park, "Application of metasurfaces in the design of performance enhanced low-profile antennas," *EPJ Appl. Metamater.*, vol. 5, p. 11, Dec. 2018.
[6] S. X. Ta and I. Park, "Artificial magnetic conductor-based circularly polarized crossed-dipole antennas: 2. AMC structure without grounding pins," *Radio Sci.*, vol. 52, pp. 642–652, May 2017.
[7] W. Chaihongsa, R. Kuse, K. Furuya, C. Phongcharoenpanich, and T. Fukusako, "Broadband linear-to-circular polarisation conversion using the diamond-shaped reflecting metasurface," *IET Microw. Antennas Propag.*, vol. 14, no. 9, pp. 943–949, Jul. 2020.
[8] W. Yang, J. Zhou, Z. Yu, and L. Li, "Single-fed low profile broadband circularly polarized stacked patch antenna," *IEEE Trans. Antennas Propag.*, vol. 62, no. 10, pp. 5406–5410, Oct. 2014.
[9] S. Ye, J. Geng, X. Liang, Y. J. Guo, and R. Jin, "A compact dual-band orthogonal circularly polarized antenna array with disparate elements," *IEEE Trans. Antennas Propag.*, vol. 63, no. 4, pp. 1359–1364, Apr. 2015.
[10] K. Agarwal, Nasimuddin, and A. Alphones, "Wideband circularly polarized AMC reflector backed aperture antenna," *IEEE Trans. Antennas Propag.*, vol. 61, no. 3, pp. 1456–1461, Mar. 2013.
[11] S. X. Ta and I. Park, "Low-profile broadband circularly polarized patch antenna using metasurface," *IEEE Trans. Antennas Propag.*, vol. 63, no. 12, pp. 5929–5934, Dec. 2015.
[12] Nasimuddin, X. Qing, and Z. N. Chen, "Metasurface-based low profile broadband circularly polarized antenna," in *Proc. IEEE Region Conf. (TENCON)*, Penang, Malaysia, Nov. 2017, pp. 2378–2382.
[13] H. H. Tran and I. Park, "A dual-wideband circularly polarized antenna using an artificial magnetic conductor," *IEEE Antennas Wireless Propag. Lett.*, vol. 15, pp. 950–953, 2016.
[14] S. Maruyama and T. Fukusako, "An interpretative study on circularly polarized patch antenna using artificial ground structure," *IEEE Trans. Antennas Propag.*, vol. 62, no. 11, pp. 5919–5924, Nov. 2014.
[15] Y. Kai and T. Fukusako, "Broadband circularly polarized patch antenna with low crosspolarization using artificial ground structure," *Microw. Opt. Technol. Lett.*, vol. 60, no. 4, pp. 840–845, Apr. 2018.
[16] T. Fukusako and R. Kuse, "Metasurface designs for wideband circularly polarized patch antennas: A review and an interpretative study," in *Proc. IEEE Asia–Pacific Microw. Conf. (APMC2020),* Hong Kong SAR, China, Dec. 2020, pp. 125–127.
[17] K. Pookkapund, A. Sakonkanapong, R. Kuse, C. Phongcharoenpanich, and T. Fukusako, "Broadband circularly polarized microstrip patch antenna using circular artificial ground structure and meandering probe," *IEEE Access*, vol. 8, pp. 173854–173864, 2020.
[18] R. Remski, "Analysis of photonic bandgap surfaces using Ansoft HFSS," *Microw. J. Euro Global Ed.*, vol. 43, no. 9, pp. 190–199, Sep. 2000.
[19] F. Yang and Y. Rahmat-Samii, "A low profile single dipole antenna radiating circularly polarized waves," *IEEE Trans. Antennas Propag.*, vol. 53, no. 9, pp. 3083–3086, Sep. 2005.
[20] H.-W. Lai and K.-M. Luk, "Design and study of wide-band patch antenna fed by meandering probe," *IEEE Trans. Antennas Propag.*, vol. 54, no. 2, pp. 564–571, Feb. 2006.
[21] Q. W. Lin, H. Wong, X. Y. Zhang, and H. W. Lai, "Printed meandering probe-fed circularly polarized patch antenna with wide bandwidth," *IEEE Antennas Wireless Propag. Lett.*, vol. 13, pp. 654–657, 2014.
[22] D. M. Pozar, "Radiation and scattering from a microstrip patch on a uniaxial substrate," *IEEE Trans. Antennas Propag.*, vol. 35, no. 6, pp. 613–621, Jun. 1987.
[23] T. A. Miligan, *Modern Antenna Design*. Hoboken, NJ, USA: IEEE Press, 2005.

UUGANBAYAR PUREVDORJ (Graduate Student Member, IEEE) was born in Govi-Altai, Mongolia, in 1987. He received the B.S. and M.S. degrees in engineering from the Mongolian University of Science and Technology (MUST) in 2009 and 2011, respectively. He is currently pursuing the Ph.D. degree with Kumamoto University, Japan. He joined MUST as an Instructor in 2011. His research interests include advanced wireless networks, microwave and antenna design, and their applications.

RYUJI KUSE (Member, IEEE) received the B.E., M.E., and Ph.D. degrees in engineering from Fukui University, Fukui, Japan, in 2011, 2013, and 2016, respectively. In 2017, he joined Kumamoto University, Kumamoto, Japan, as an Assistant Professor, where he is currently working with the Department of Computer Science and Electrical Engineering. His research interests include metasurfaces, MIMO antennas, circularly polarized antennas, and their applications. He is a member of IEICE.

TAKESHI FUKUSAKO (Senior Member, IEEE) received the B.E., M.E., and Ph.D. degrees in engineering from the Kyoto Institute of Technology, Kyoto, Japan, in 1992, 1994, and 1997, respectively. In 1997, he joined Kumamoto University, Kumamoto, Japan, as a Research Associate, where he is currently working as a Professor with the Department of Computer Science and Electrical Engineering. From 2005 to 2006, he was a Visiting Researcher with the University of Manitoba, Winnipeg, MN, Canada. He was a Visiting Associate Professor with the City University of Hong Kong, Hong Kong, SAR, China, from March 2015 to April 2015. His current research interests include antenna design, especially broadband antennas, circularly polarized antennas, and electrically small antennas, and their applications. In 2014, he served as one of the TPC co-chairs at the 2014 IEEE International Workshop on Electromagnetics: Applications and Student Innovation Competition, and in 2017, he served as one of the general chairs at the IEEE International Conference on Computational Electromagnetics. He has served as an Associate Editor for *IEICE Transactions on Communications* from 2012 to 2016, and he has also been an Associate Editor of the IEEE TRANSACTIONS ON ANTENNAS AND PROPAGATION since 2015. He is a Senior Member of IEICE.